Sensors & Actuators: B. Chemical 380 (2023) 133394

Contents lists available at ScienceDirect

Sensors and Actuators: B. Chemical

journal homepage: www.elsevier.com/locate/snb

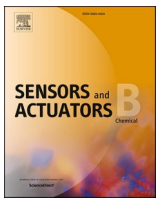

Towards the maximization of nanochannels blockage through antibody-antigen charge control: Application for the detection of an Alzheimer's disease biomarker

Celia Toyos-Rodríguez [a,b], Francisco Javier García-Alonso [b,c], Alfredo de la Escosura-Muñiz [a,b,*]

[a] NanoBioAnalysis Group-Department of Physical and Analytical Chemistry, University of Oviedo, Julián Clavería 8, 33006 Oviedo, Spain
[b] Biotechnology Institute of Asturias, University of Oviedo, Santiago Gascon Building, 33006 Oviedo, Spain
[c] NanoBioAnalysis Group-Department of Organic and Inorganic Chemistry, University of Oviedo, Julián Clavería 8, 33006 Oviedo, Spain

ARTICLE INFO

Keywords:
Nanochannels
Nanopores
Biosensor
Tau protein
Alzheimer's disease

ABSTRACT

Although size and charge effects in nanochannels have been previously approached for electrochemical immunosensing, as far as we know, thorough studies on the effect of both the antibody and the antibody/antigen immunocomplex charges at different pHs have not been deeply reported. In this context, we present here an unprecedented study of such parameters, applied also for the first time for the detection of an Alzheimer's disease (AD) biomarker. AD detection is currently based in time consuming and expensive techniques, so that the development of alternative analytical strategies for facilitating its diagnosis is still a need. To reach that purpose, we propose here the development of a nanochannel-based system for the electrochemical monitoring of Tau protein, an important AD biomarker. Tau protein is selectively captured by specific antibodies immobilized in the inner walls of the nanochannels of nanoporous alumina membranes. The captured Tau protein blocks the nanochannel and difficulties the passage of red-ox indicator ions, which is voltammetrically monitored using an indium tin oxide/poly(ethylene terephthalate) (ITO/PET) electrode as transducer. The charges of both the antibody and the Tau antigen at different pHs and their effect on the diffusion of the red-ox indicator ions to the electrode are carefully evaluated to maximize the electrostatic blocking of the nanochannels upon the immunocomplex formation. The developed biosensing system allows the determination of Tau protein with a detection limit of 4.3 ng/mL, which is within the range of clinical interest, showing also excellent recovery percentages in human plasma samples.

1. Introduction

Neurodegenerative diseases are multifactorial pathologies that act on the central and peripheral nervous system [1]. The incidence of these pathologies increases among age, so that the rise in life expectancy is expected to worsen their burden [2]. From all of them, Alzheimer's disease (AD) is the most common, affecting 30% of people older than 85 years, a value that is increasing in a 6–8% yearly [3,4]. AD neurodegeneration manifests at initial stages with episodes of memory loss and evolves to deterioration in cognition, temporal space disorientation and the incapacity to carry out quotidian activities [5,6].

The incapacitating condition of this pathology has also a relevant impact both socially and economically, with a burden of €232 billion in 2015 [7].

For that reason, a rapid detection is a major concern and, in this process, AD biomarkers, between which Tau protein is included, have been identified as a research priority [8].

Tau protein plays a pivotal role in the development of several neurodegenerative diseases, known as tauopathies [9]. AD, frontotemporal lobar dementia (FTD) [10] or corticobasal degeneration (CBD) are some of them. In the case of AD, Tau is related with the formation of neurofibrillary tangles (NFTs) [11]. All of it, constitutes Tau as a common pathological hallmark in neurodegeneration, so that its detection is desirable for the sensitive diagnosis of AD and other neurodegenerative disorders.

Tau proteins acts as a neuronal microtubule-associated protein that

* Corresponding author at: NanoBioAnalysis Group-Department of Physical and Analytical Chemistry, University of Oviedo, Julián Clavería 8, 33006 Oviedo, Spain.
E-mail address: alfredo.escosura@uniovi.es (A. de la Escosura-Muñiz).

https://doi.org/10.1016/j.snb.2023.133394
Received 7 November 2022; Received in revised form 22 December 2022; Accepted 18 January 2023
Available online 19 January 2023

regulates axonal growth and neuronal polarity, as it is mainly found associated to axons [12]. In the normal human brain, Tau regulates the assembly of tubulin into microtubules [13]. This regulation is mediated by the phosphorylation of Tau protein, however, an hyperphosphorylation of this protein increases its tendency to aggregate and to assemble into pair helical filaments (PHFs) and later in the formation of intracellular NFTs, highly related with AD [14–17]. The formation of NFTs has also been related with ß-amyloid (Aß), a relevant AD biomarker [18], as according to the amyloid cascade hypothesis [19], Tau hyperphosphorylation occurs following (Aß) deposition [20,21].

Current Tau protein detection is based on enzyme-linked immunosorbent assay (ELISA), mass spectrometry or surface plasmon resonance among other techniques [22–24]. But these procedures are time-consuming and expensive, so that they are not suitable for their use as generalized screening methods. For that reason, the development of optical and electrochemical biosensors for the detection of AD biomarkers has increased among the last years, obtaining promising results [25,26]. However, most of these approaches are based on sandwich-based or competitive assays, depending on the analyte size, requiring the use of labels. The complexity of these procedures is meant to be reduced by the implementation of label-free strategies, for what the use of nanochannels as biosensing platforms stands out [27,28].

In the 50's Wallace Coulter developed the first microchannel-based biosensing device [29]. The mechanism of action of this system is based on the detection of changes in the electrical conductance between two chambers connected by a microchannel when an analyte passes through it. From this first device, several improvements have been done until reaching nanometer channel systems [30], able to detect biomolecules as ssDNA following the so-called stochastic sensing [27,31].

In the development of nanochannel-based systems, the use of naturally pore forming biomolecules such as pore forming toxins has also been exploited [31,32]. However, these biological systems in occasions lack from stability and are suitable just for small size molecules, so that alternative systems such as solid-state nanochannels have been postulated [33]. As an example of them, nanoporous alumina membranes show up. They are characterized by having reduced pore sizes while maintaining an enhanced pore density, what increases the available surface area [34]. These membranes have already been used for the electrochemical detection of proteins [35], DNA [36], enzymes [37] or *in situ* monitoring of cell secreted proteins [38] and anti-virulence agents [39], using screen printed carbon electrodes (SPCEs) or indium tin oxide/poly(ethylene terephthalate) (ITO/PET) electrodes. The excellent filtering properties and low unspecific adsorption of proteins shown by this material has made it ideal for the analysis of samples with complex matrixes. However, the detection of AD biomarkers is seldom studied within nanochannels [40].

In this context, we propose here a novel approach for the detection of Tau protein using nanoporous alumina membranes as sensing platforms and ITO/PET electrodes as transducers. The analytical detection technique used is based on the blockage of the signal, both steric and electrostatic, due to the presence of increasing concentrations of Tau protein, captured by specific antibodies. Moreover, the effect of the pH in the blockage capacity and the performance in real plasma samples has also been investigated. The developed biosensor is the first approach, to our knowledge, in which nanochannels are used for Tau protein detection.

2. Materials and methods

2.1. Reagents and equipment

(3-aminopropyl) triethoxysilane (APTES), amyloid beta protein (ß-amyloid), avidin from egg white, bovine serum albumin (BSA), N-(3-Dimethylaminopropyl)-N′-ethylcarbodiimide hydrochloride (EDC), N-Hydroxysulfosuccinimide sodium salt (sulfo-NHS), Tau-441 (1−441) protein, plasma from human (prepared from donors pooled blood), potassium ferrocyanide $K_4[Fe(CN)_6]$, (2-(N-morpholino) ethanesulfonic acid) (MES) and Tris (tris(hydroxymethyl) aminomethane)-HCl (Tris-HCl) were purchased from Sigma-Aldrich (Spain). Anti-Tau monoclonal antibody (BT2) was purchased from Thermo Fisher Scientific (Spain).

Buffer solutions used were 0.1 M MES pH 5.0, and 0.1 M Tris-HCl at pH 6.5, 7.2 and 9.0 and they were all prepared in ultrapure water (18.2 MΩ·cm @ 25 ºC) obtained from a Millipore Direct-Q® 3 UV purification system from Millipore Ibérica S.A (Spain).

Nanoporous alumina membranes (Whatman® AnodiscTM filters, 13 mm diameter, 60 µm thickness, 100 nm pore) were obtained from VWR International Eurolabs (Spain). ITO/PET sheets (surface resistivity 60 Ω/sq) were obtained from Sigma-Aldrich (Spain). ITO/PET was used in pieces of 43 × 20 mm as electrochemical transducers. As reference electrode a silver/silver chloride from CH Instruments, Inc (United States of America) was used, while a platinum wire from Alfa Aesar (United States of America) was selected as counter electrode.

The electrochemical measurements were performed inside a methacrylate electrochemical cell using an Autolab PGSTAT-10 (Eco Chemie (Netherlands)) connected to a PC and controlled by Autolab GPES software. The nanoporous membranes were characterized using a scanning electron microscope (SEM) MEB JOEL-6100 (Japan).

2.2. Methods

2.2.1. Nanoporous alumina membranes functionalization and anti-Tau antibody immobilization

Anti-Tau antibodies were immobilized in the inner walls of the nanochannels of the nanoporous alumina membranes following a previously optimized procedure, consisting in the functionalization of the alumina with amino groups through a silanization protocol, followed by the immobilization of the antibody through the peptide bond, using the EDC/NHS chemistry (see Fig. S1 at the Supplementary Material) [41].

Briefly, nanoporous membranes were immersed in ultrapure water and boiled for 1 h. This boiling step is done both for cleaning them and activate the hydroxyl groups present in the surface, what favours the latter silanization process. [42]. Then, the membranes were dried under a nitrogen flow and then plunged into a 5% APTES solution in acetone for 1 h. The solution was withdrawn, and the membranes were washed three times with pure acetone. After that, they were dried at 120ºC for 30 min. After this process, the silanized membranes could be stored for weeks without losing their activity.

For the optimization of the immobilization of anti-Tau antibodies in the inner wall of the nanochannels, 30 µL of a solution of 5 mM EDC/sulfo-NHS in MES pH 5, containing different concentrations of the anti-Tau antibody (0.5, 1, 10 and 50 µg/mL) were placed on the top side of the membrane and left at room temperature for incubation for 2 h. Control assays were performed in Tris-HCl 10 mM pH 7.00 without antibody being added. After this incubation, membranes were placed on top of a rack and gently washed with Tris-HCl 10 mM pH 7.00 buffer (see Fig. S2 at the Supplementary Material).

2.2.2. Immunoassay for Tau capturing in the nanochannels

For that purpose, 30 µL of solutions containing increasing concentrations of Tau protein (5–100 ng/mL) were placed on the membranes and left for incubation at room temperature during 3 h. Then, membranes were put on top of a rack and thoroughly cleaned with Tris-HCl 10 mM. To achieve an enhanced variation between control samples and Tau-containing ones, pH of the final buffer solution used for cleaning and measuring was adjusted, thus trying at pH 7.00, 8.24 and 9.00. Control assays were performed using the same procedure but without the addition of Tau protein.

To evaluate the selectivity of the developed sensor, the above-described methodology was followed for 100 ng/mL solutions of ß-amyloid, avidin and BSA solutions instead of that of Tau protein.

Long-term stability of the membranes was also evaluated by storing a set of anti-Tau antibody modified membranes at 4ºC for one month and

adding a 100 ng/mL Tau solution at different time points.

2.2.3. Cell set-up and electrochemical measurements

The electrochemical measurements were performed fixing the nanoporous membrane on top of an ITO/PET electrode, using a methacrylate cell. First, the membrane was placed with the filtering side up on top of the conductive side of the ITO/PET electrode. The electrode was introduced between two pieces of methacrylate, one of them with a hole that delimitates the ITO/PET working electrode area and the electrochemical cell. Then, the whole system was adjusted with screws to avoid liquid leakage. Ag/AgCl and a Pt wire were used as reference and counter electrodes respectively.

For the electrochemical measurement, the electrochemical cell was filled with 400 μL of a 10 mM solution of $K_4[Fe(CN)_6]$ red-ox indicator. Then, a pre-treatment at − 0.55 V was applied for 30 s and immediately after, a differential pulse voltammetric (DPV) scan between + 0.1 V and + 1.3 V was done applying a step potential of 10 mV, a modulation amplitude of 50 mV and at a scan rate of 33.5 mV/s. As a result, the oxidation of $[Fe(CN)_6]^{4-}$ to $[Fe(CN)_6]^{3-}$ was observed and the correspondent peak current at approximately + 0.6 V was selected as analytical signal.

Measurements were performed in triplicate, using different nanoporous alumina membranes and ITO/PET electrodes.

The whole time required for performing the analysis (from the step of adding the sample containing the antigen), including also mounting the cell, is of around 4 h (for 20 membranes: analysis of 20 samples) or 6 h (for 60 membranes: analysis of 60 samples). Using more cells simultaneously, the number of analysis could be further increased, estimating 1 h more per each 20 membranes (i.e. 8 h for analysing 100 samples).

2.2.4. Spike and recovery assay

Spike and recovery is fundamental for the evaluation of the performance of a biosensor in complex samples. A plasma sample from healthy patients was used for such purpose. This experiment was performed by spiking the plasma sample with different concentrations (5 and 25 ng/mL) of Tau protein (n = 3 for each sample). Then, the spiked samples were evaluated in the nanochannels-based sensing system, being finally calculated the % of recovery of the analytical sample in plasma, compared with the obtained in non-spiked plasma.

3. Results and discussion

3.1. Sensing principle for Tau protein detection: optimization of the main parameters involved

In this work, commercial nanoporous alumina membranes with a nominal pore diameter of 100 nm (real average diameter of 108 ± 16 nm, Fig. S3 at the Supplementary Material) were selected as sensing platforms due to their easy functionalization, filtering capacities and low unspecific adsorption of proteins. Membranes were first characterized by scanning electron microscopy showing a regular and well dispersed morphology (Fig. 1A).

The principle of the developed biosensor is based on the nanochannels blocking by the Tau protein captured by the specific antibody. In the presence of this protein, the flow of the $[Fe(CN)_6]^{4-}$ red-ox indicator through the nanochannels is reduced, due to both steric and electrostatic impediments (Fig. 1B). This is monitored through the decrease in the voltammetric oxidation of $[Fe(CN)_6]^{4-}$ to $[Fe(CN)_6]^{3-}$ which is evaluated using the electrochemical set-up detailed at *methods* section, with ITO/PET working electrodes (Fig. 1C). Compared to screen-printed carbon electrodes (SPCEs), previously used together with

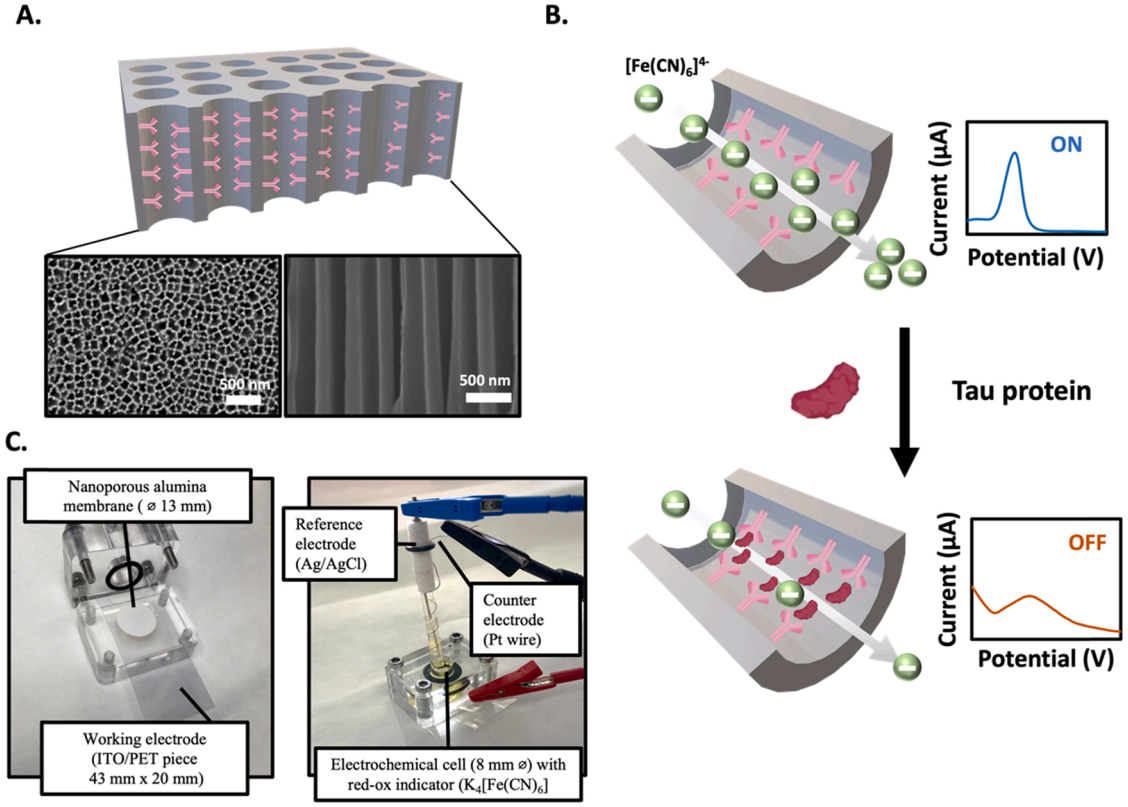

Fig. 1. A. Schematic representation of the pore distribution inside a nanoporous alumina membrane accompanied by SEM micrographs of both top view (left) and cross- section view (right) of the membranes. B. Schematic representation of the principle of the biosensor developed, based on the nanochannels blocking by the Tau protein captured by specific antibodies, which hinders the diffusion of $[Fe(CN)_6]^{4-}$ to the electrode, leading to a decrease in its voltammetric oxidation to $[Fe(CN)_6]^{3-}$. C. Electrochemical set-up used in this sensing device.

nanoporous alumina membranes in nanochannels-based electrochemical biosensing systems [43], ITO/PET electrodes show important advantages for such particular application. The use of SPCEs as transducers in these systems suffered from important limitations related to: (i) the membrane covers the three electrodes (reference, counter and working), inducing not wanted blocking of the reference electrode, which leads to unstable signals; (ii) the roughness of the working carbon electrode makes difficult the assembling with the membrane, leading to irreproducibility in the signals. In contrast, our experimental set-up allows to improve the system performance, overcoming such limitations. The flatter surface of the ITO/PET electrode allows to improve the membrane/electrode assembling and consequently the system reproducibility. The use of external counter and reference electrodes avoids the electrodes blocking with the membrane, giving much more stable signals. Moreover, the flexibility and biocompatibility of the ITO/PET make it ideal for future applications in wearable electrochemical sensing [44].

3.1.1. *Optimization of anti-Tau antibody concentration*

As detailed in *methods* section, anti-Tau antibodies are immobilized in the inner walls of the nanochannels through the peptide bond, taking advantage of the carbodiimide chemistry. The minimum concentration for a total covering of the nanochannels surface was evaluated by monitoring the certain blocking effect that the antibodies by themselves exert toward the diffusion of the red-ox indicator ion through to the electrode. This blockage could be associated to both steric and electrostatic effects, as the size of an antibody is considered to be around 10–15 nm [45,46], while the size of the ions of $[Fe(CN)_6]^{4-}$ is lower than 1 nm.

Therefore, the first step performed was the immobilization of different anti-Tau antibody concentrations to study the blockage produced. The degree of blockage in the signal has been calculated as described in Eq. 1:

$$\text{Index of Antibody Current Blockage } (\Delta I_{ab})\ (\%) = \left(\frac{I_0 \text{bare membrane} - I \text{ antibody modified membrane}}{I_0 \text{ bare membrane}}\right) x100 \quad (1)$$

where I is the value of the peak current corresponding to the voltammetric oxidation of $[Fe(CN)_6]^{4-}$ to $[Fe(CN)_6]^{3-}$. The use of this parameter as analytical signal in this experiment has helped to normalize the results and obtain a better conclusion.

Anti-Tau antibody in concentrations ranging from 0.5 to 50 μg/mL was evaluated. The isoelectric point (pI) of the antibody is a key parameter for the selection of the adequate buffer in which the $[Fe(CN)_6]^{4-}$ red-ox indicator solution is prepared. Previous experiments have confirmed that the pI for Tau antibodies is between 5 and 8 [47] but these values could vary depending on the species in which the antibody has been generated. In this regard, the monoclonal anti-Tau antibody used in this work has been produced in mouse, being the antibody an IgG1 kappa light chain that is associated with a pI of 6.4 [48].

In view of this information, and with the aim of taking advantage of the electrostatic hindrance for this optimization, a Tris-HCl buffer at pH

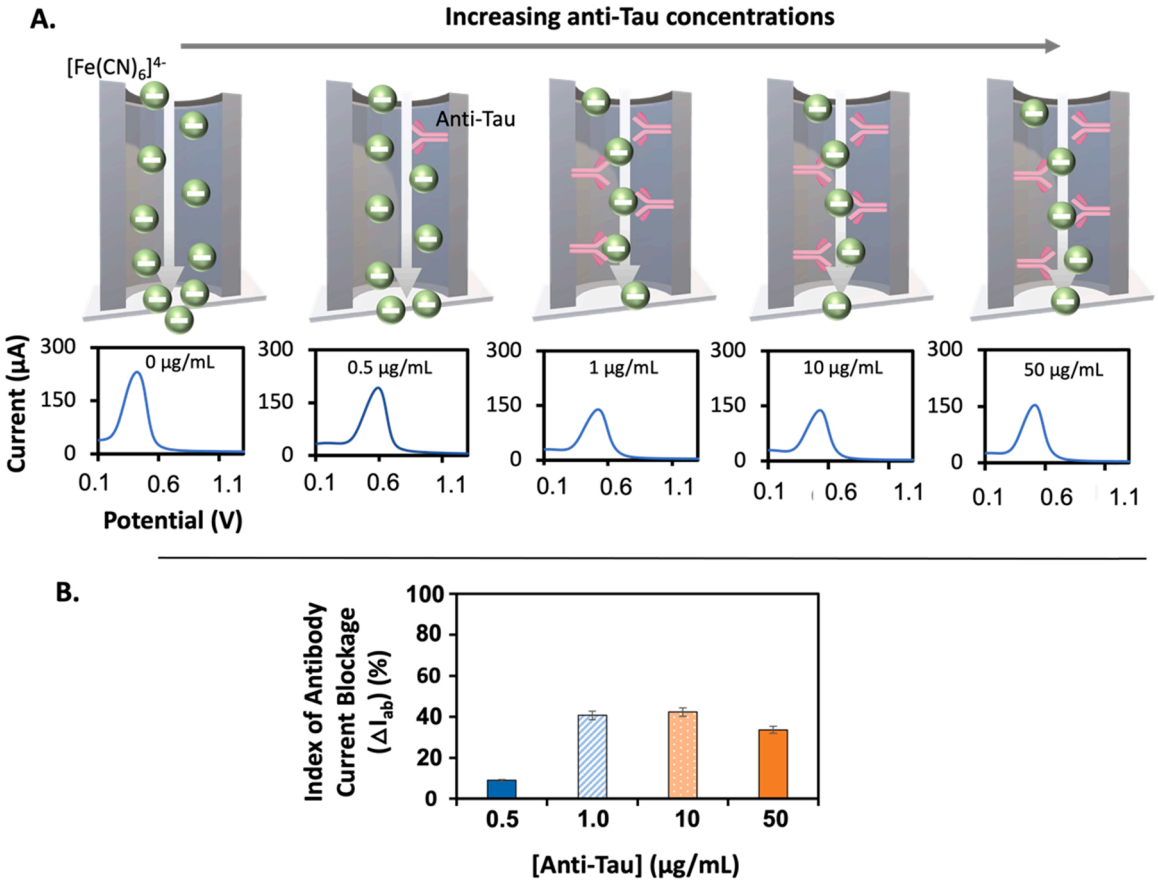

Fig. 2. Optimization of the concentration of anti-Tau antibody immobilized inside the nanochannels. A. (Up) Schematic illustration of the different situations with different amounts of antibody immobilized and the blockage on the diffusion of the $[Fe(CN)_6]^{4-}$ red-ox indicator ions; (Down) Differential pulse voltammograms (DPV) recorded for each concentration of anti-tau antibody concentration evaluated, using a 10 mM $K_4[Fe(CN)_6]$ solution in 10 mM Tris-HCl buffer at pH 7.00, applying a pre-concentration potential of − 0.55 V for 30 s and scanning from + 0.1 V to + 1.3 V at a step potential of 10 mV, a modulation amplitude of 50 mV and a scan rate of 33.5 mV/s; B. Comparative representation of the index of antibody current blockage (as defined in Eq. 1) for different anti-Tau antibody concentrations. Data are given as average ± SD (n = 3).

of 7.00 was selected as $[Fe(CN)_6]^{4-}$ solution media, so as to have the antibodies negatively charged which should exert a certain repulsion to the diffusion of the $[Fe(CN)_6]^{4-}$ ions. This is translated into an increased blockage of the analytical signal. By selecting this pH, a further confirmation of the pI of the antibody could be done in an easy-to-manage form.

As shown and illustrated in Fig. 2A, the increasing amount of anti-Tau antibody produces a gradual decrease in the voltammetric signal, reaching a saturation for 1 μg/mL. This behaviour is consistent with our hypothesis, suggesting that the presence of the negatively charged antibodies is hindering the diffusion of the negatively charged red-ox indicator ions. In terms of blockage in the signal (Fig. 2B) at a concentration of 0.5 μg/mL the index of blockage produced is of 9% while this value is notably enlarged to 41% with a slight increase in the concentration to 1 μg/mL. This value is maintained at higher concentrations, reaching 42% for 10 μg/mL, what indicates that the saturation of the nanochannels has been achieved and the increase in anti-Tau antibody concentration is not translated into a greater immobilization of them inside the nanochannel. The slight decrease to 34% observed for 50 μg/mL is probably due to the saturation of the signal. These results suggest that the minimum amount of anti-Tau antibody giving the total covering of the nanochannels corresponds to a concentration of 1 μg/mL, which was selected as optimum for the development of the immunoassay.

3.1.2. *Immunoassay for Tau protein capturing inside the channels and optimization of the pH of the measuring buffer*

After the optimization of the anti-Tau antibody concentration, immunoassays were performed for Tau protein capturing inside the nanochannels. The Tau protein molecule has a size of 69–75 nm in a non-phosphorylated form while this value slightly increases in a hyperphosphorylated form [49]. Considering the presence of anti-Tau antibodies (of around 10–15 nm) in the inner walls of the nanochannels (real average diameter of 108 nm), the capturing of the Tau protein would highly increase the steric blockage of the signal, still allowing the $[Fe(CN)_6]^{4-}$ red-ox indicator ions diffusion.

Moreover, proteins may have a positive or negative external net charge depending on the pH of the measurement solution. This charge will contribute to the signal blockage by electrostatic interactions of the nanochannel due to charge repulsion between the negative ions of the red-ox indicator and the biomolecule. For that reason, to have the maximum blockage by low concentrations of Tau protein, the optimum pH for the buffer used during measurements was evaluated.

In this experiment, a fixed concentration of Tau protein of 100 ng/mL was used. Tau protein behaves as a dipole containing two domains, a N-terminal region which has a pI of 3.8, and a C-terminal region with a pI of 10.8. Tau protein also contains a proline-rich domain with a pI of 11.4. However, posttranslational modifications of this protein could clearly modulate these dipoles [50]. For that reason, the use of a measuring pH that allows to detect a wider range of Tau protein forms is desirable for the real implementation of the biosensor developed in this work for further clinical samples analysis.

In this work, the model Tau-441, recombinant protein, the longest human brain Tau isoform (441 amino acids) was used [51]. The pI value for Tau-441 used was also theoretically calculated using ProtParam tool following previously published procedures (see Fig. S4 at the Supplementary Material) [50,52], providing a pI value of 8.24 which correlates with previously reported values [53].

Taking into consideration this information, pH values of 7.00, 8.24 and 9.00 were used for preparing the 10 mM $K_4[Fe(CN)_6]$ red-ox indicator solutions for studying the effect of the pH in the nanochannels blockage, as defined in Eq. 2:

$$\text{Index of Tau Current Blockage } (\Delta I_{Tau})\ (\%) = \left(\frac{I_0 \text{ antibody modified membrane} - \text{Iimmunoassay}}{I_0 \text{ antibody modified membrane}}\right) x100 \quad (2)$$

It is worthy to mention that according to the pI of the anti-Tau antibodies, they should remain negatively charged for all the pH values evaluated, being their inherent blockage effect considered as a constant background which does not affect the biosensing system.

According to the scheme represented in Fig. 3A at a pH of 8.24, equivalent to the pI of Tau-441, the protein molecules are uncharged, so not electrostatic effects should be induced by the presence of the protein inside the nanochannels. However, a noticeable blockage in the current up to a 32% index (as defined in Eq. 2) is measured, suggesting that steric impediments (size above 69–75 nm in a nanochannel of 100 nm in diameter) have an important contribution in hindering the diffusion of the red-ox indicator ions.

At a pH of 7.00, which is below the pI value of Tau-441, the net charge of the protein is positive, so this should induce an electrostatic attraction effect to the $[Fe(CN)_6]^{4-}$ ions and consequently an increase in the voltammetric signal. This is corroborated by the decrease in the blockage index (18%) obtained, as depicted in Fig. 3B, induced by the steric blockage of the protein (size above 69–75 nm in a nanochannel of 100 nm in diameter).

Interestingly, increasing the pH to 9.00, a value which is higher than the pI of the Tau-441, the protein is negatively charged, impeding the diffusion of the $[Fe(CN)_6]^{4-}$ ions. This leads to a dramatic increase in the current blockage index to 73% (Fig. 3B). According to these results, pH 9.00 is selected as the optimum value for obtaining the maximum response regarding the analytical signal. Moreover, this pH value allows to cover a wide spectrum of pIs, so that all variants of Tau protein, independently of their phosphorylation state and isoform, could be detected with a high precision. The quite basic pH does not significantly affect the chemical stability of the ferro/ferrycyanide pair as it has been previously stated that this redox molecule retains its activity even at pH 14 [54]. Although a small decrease in the analytical signal is recorded at pH 9.00, compared to measurements at pH 7.00, the use of normalized blocking indexes eliminates the impact of these small variations in the result, facilitating comparison between different conditions.

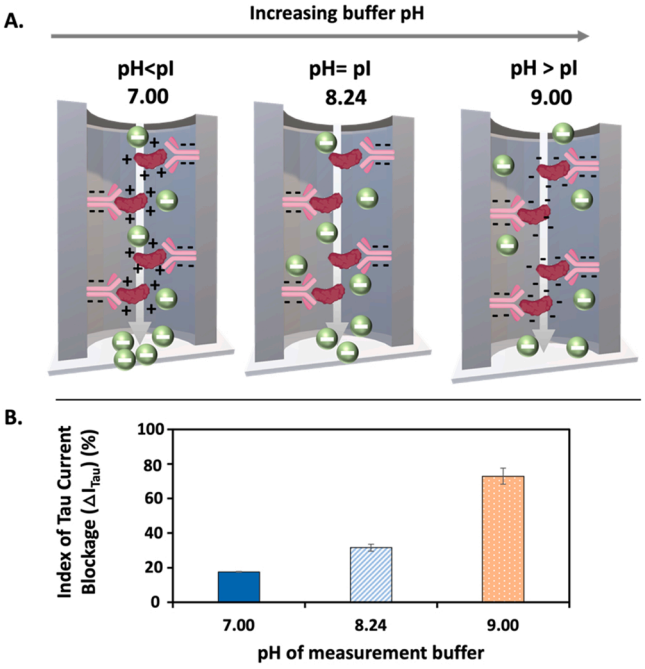

Fig. 3. Effect of the pH of the measurement buffer in the analytical system. A. Representation of the different charges of both anti-Tau antibody and Tau protein depending on the pH of the measurement solution and how it affects the diffusion of the $[Fe(CN)_6]^{4-}$ red-ox indicator ions through the channel; B. Effect of the pH on the index of Tau current blockage (as defined in Eq. 2) represented by the average ± SD (n = 3).

3.2. Electrochemical detection of Tau protein

After the optimization of the main parameters involved in the detection of Tau protein, the biosensor developed was used for the determination of different concentrations of this biomarker. The Tau protein incubation is performed at a pH 7.00, as the immunoreaction has been proved to be more efficient and stable at such pH value [55]. After this incubation step, electrochemical measurements are performed using a $[Fe(CN)_6]^{4-}$ redox solution in a buffer at pH 9.00. At this pH value, the Tau protein is negatively charged, what optimizes the blockage obtained, as proved in previous sections. Due to the short duration of the measurement, the chemical stability of the antigen-antibody interaction should not be compromised at such basic pH.

As expected, the presence of increasing concentrations of Tau protein leads to a decrease in the voltammetric peak current corresponding to the oxidation of the red-ox indicator $[Fe(CN)_6]^{4-}$ to $[Fe(CN)_6]^{3-}$ at approximately + 0.6 V (Fig. 4A), which is the analytical signal selected for the quantitative analysis. It was found a linear relationship between such analytical signal and the Tau protein concentration within the range 5–100 ng/mL (Fig. 4B) with a correlation coefficient (r) of 0.9981, adjusted to this equation:

$$\text{Peak current } (\mu A) = -0{,}112\ [\text{Tau}]\ (\text{ng/mL}) + 20{,}4 \quad (3)$$

The biosensing system developed has a limit of detection (LOD, calculated as three times the standard deviation of the intercepted divided by the slope) of 4.32 ng/mL and an appropriate reproducibility with a relative standard deviation (RSD) of 9%. Although there is a quite controversy in the bibliography on the expected levels of Tau protein in plasma of both healthy and AD patients, in the particular case of the immunoassays, the literature suggests that the found Tau levels strongly depend on the specific anti-Tau antibody used. Some reported immunoassays [56] have shown that the Tau protein is present in AD patients plasma at levels of around 60 ng/mL, which are above the detection limit of our immunoassay. This suggests that our methodology is potentially suitable for the determination of Tau protein in the real scenario. Anyway, a careful evaluation of different antibodies may be necessary for the real implementation of this technology.

Our methodology is faster and cheaper than ELISA kits, since neither competitive assays nor the use of labels are required. Moreover, our approach benefits of the low cost and portability of the potentiostats used for the electrochemical detection [57], which is ideal for a point-of-care detection of Alzheimer's disease.

3.3. System selectivity and long-term stability

Selectivity of the biosensor was evaluated against common analytes present in human samples, as ß-amyloid, another common AD biomarker, avidin and BSA (Fig. 4C). It has been observed that the blockage produced in the presence of the abovementioned analytes is lower than 20%, what supposes an irrelevant value compared to the one obtained by Tau protein (61%), proving the selectivity of the method.

Additionally, long-term stability of the developed sensor has been preliminary addressed by storing a set of anti-Tau antibody modified membranes at 4ºC for one month and evaluating the response for a 100 ng/mL Tau solution at different time points. As shown at the Supplementary Material (Fig. S5), the response of the system was stable and reproducible for at least 21 days, noticing a decrease after 30 days of storage. Although this aspect requires further optimization, the preliminary stability observed suggests that the antibody-modified membranes could be stored ready for the sample analysis, which would only involve the steps of the sample incubation on the membrane, washing and measuring buffer adding.

3.4. System performance in real samples

Tau protein is well-known to be a suitable biomarker for the detection of AD and other neurodegenerative disorders, as high levels of this protein are present in cerebrospinal fluid (CSF) and plasma samples of patients with different pathologies [58].

The main obstacle to overcome for measuring Tau protein is the

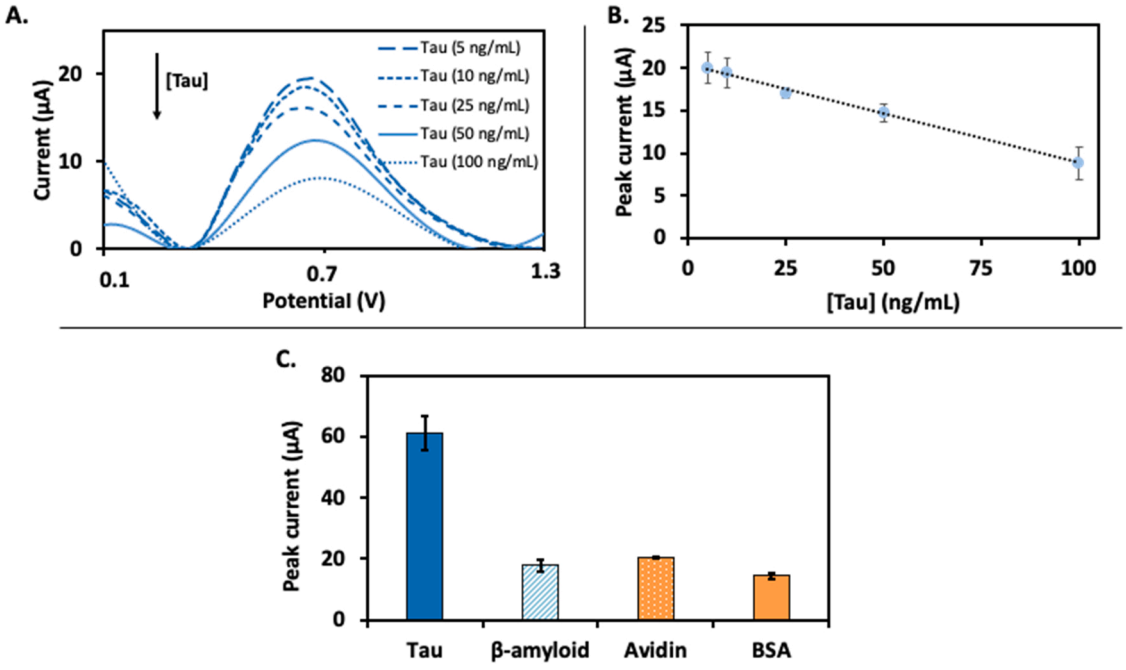

Fig. 4. Tau protein detection through antibody recognition inside the nanochannels. A. Differential pulse voltammograms (DPV) recorded for different Tau concentrations, using as red-ox indicator 10 mM $K_4[Fe(CN)_6]$ in buffer at pH 9.00. Anti-Tau antibody concentration: 1 µg/mL. Pre-concentration potential: − 0.55 V for 30 s; scan range: + 0.1 V to + 1.3 V; step potential: 10 mV; modulation amplitude: 50 mV; scan rate: 33.5 mV/s. B. Calibration curve obtained by representing the analytical signal (value of the peak current at +0.6 V) ± SD (n = 3), obtained for the different concentrations of Tau protein assayed. C. Selectivity assay using a concentration of 100 ng/mL of Tau protein, ß-amyloid, avidin or BSA.

complexity of real samples as possible interferences could occur [59,60]. For addressing this drawback, nanoporous alumina membranes are suitable platforms, as it is well known that this material has a low protein adsorption rate, acting as efficient filter in complex matrixes [41, 43].

For evaluating this issue, a spike and recovery procedure was performed in plasma samples adding different Tau concentrations spiked in commercial plasma from healthy patients. The plasma samples are then added, in substitution of Tau protein dissolved in buffer solution, in the incubation step. After that a 10 mM $K_4[Fe(CN)_6]$ in buffer at pH 9.00 red-ox solution was used for measuring the decrease in current produced by Tau protein, hence assuring that both antibody and antigen are negatively charged and maximizing electrostatic blockage. The spiked assay showed an excellent recovery rate at levels around 95% (Table 1). These results clarify that the performance of the biosensor is not altered by the presence of interfering compounds, thus opening the way to its use for the detection of AD.

4. Conclusions

Tau protein, a well-known AD biomarker, has been detected in this work using a novel nanochannel-based platform. The mechanism of this biosensor is based on the voltammetric determination of the blockage that Tau protein produces to the diffusion of the red-ox indicator $[Fe(CN)_6]^{4-}$. It was already known that both steric and electrostatic interactions affect the nanochannel blockage obtained, but the contribution of both components of the antigen-antibody pair used in nanochannels-based immunosensors was less research. Our findings confirm that the control of the charge of both components by changing the buffer measurement pH is required to maximize the blockage upon the immunocomplex formation. Considering antibody pI is particularly crucial not only for the overall blockage obtained but also to properly select the antibody concentration required in the immunoassay, reducing the concentration needed and thus the immunosensor cost.

In the main, our method let detecting Tau protein with a good performance in human real samples and with a LOD of 4.3 ng/mL, which is in correlation with clinical values and with those detected by gold-standard techniques. It is worthy to mention that our methodology does not require neither labels nor competitive assays. As far as we know, this is the first time that Tau protein is detected through a nanochannel-based electrochemical sensor. This label-free sensor allows to detect Tau protein in a cheaper and faster approach, getting closer to clinical practice requirements, opening the way to a point-of-care diagnosis of AD.

Overall, our findings related the effect of both the anti-Tau antibody and the anti-Tau/Tau immunocomplex charges on the nanochannels-based biosensing system may be extended to any other antibody/antigen pair, just paying attention to the isoelectric point of such proteins, targeting applications in medicine, food analysis and environmental control among others.

CRediT authorship contribution statement

Celia Toyos-Rodríguez: Conceptualization, Experimental work, Formal analysis, Writing – original draft. **Francisco Javier García-Alonso**: Conceptualization, Supervision, Funding acquisition. **Alfredo de la Escosura-Muñiz**: Conceptualization, Data curation, Supervision, Writing – review & editing, Funding acquisition. All authors have given approval to the final version of the manuscript.

Declaration of Competing Interest

The authors declare that they have no known competing financial interests or personal relationships that could have appeared to influence the work reported in this paper.

Table 1
Spike and recovery assay data in plasma for Tau concentrations of 5 and 25 ng/mL, corresponding to the lower and medium values of the calibration curve.

Sample	Spiked Tau (ng/mL)	Current in PBS (μA)	Current in real sample (μA)	Recovery (%)
Plasma from healthy subjects	5.00	18.9	18.2	96.3
	25.0	17.0	16.3	95.6

Data Availability

Data will be made available on request.

Acknowledgements

This work has been supported by the MCI-21-PID2020-115204RB-I00 project from the Spanish Ministry of Science and Innovation (MICINN), the CTQ2017-86994-R project from the Spanish Ministry of Economy and Competitiveness (MINECO) and the SV-PA-21-AYUD/2021/51323 project from the Asturias Regional Government. C. Toyos-Rodríguez thanks the MICINN for the award of a FPI Grant (PRE2018-084953). A. de la Escosura-Muñiz also acknowledges the MICINN for the "Ramón y Cajal" Research Fellow (RyC-2016-20299).

Appendix A. Supporting information

Supplementary data associated with this article can be found in the online version at doi:10.1016/j.snb.2023.133394.

References

[1] A.D. Gitler, P. Dhillon, J. Shorter, Neurodegenerative disease: models, mechanisms, and a new hope, Dis. Model. Mech. 10 (2017) 499–502, https://doi.org/10.1242/dmm.030205.
[2] G. Deuschl, E. Beghi, F. Fazekas, T. Varga, K.A. Christoforidi, E. Sipido, C. L. Bassetti, T. Vos, V.L. Feigin, The burden of neurological diseases in Europe: an analysis for the global burden of disease study 2017, Lancet Public Health 5 (2020) e551–e567, https://doi.org/10.1016/S2468-2667(20)30190-0.
[3] H. Checkoway, J.I. Lundin, S.N. Kelada, Neurodegenerative diseases, IARC Sci. Publ. 163 (2011) 407–419.
[4] C.P. Ferri, M. Prince, C. Brayne, H. Brodaty, L. Fratiglioni, M. Ganguli, K. Hall, K. Hasegawa, H. Hendrie, Y. Huang, et al., Global prevalence of dementia: a delphi consensus study 366 (2005) 6.
[5] Alzheimer Association 2018 Alzheimer's Disease Facts and Figures; 2019; pp. 1–88;.
[6] E. Joe, J.M. Ringman, Cognitive symptoms of Alzheimer's disease: clinical management and prevention, BMJ (2019) l6217, https://doi.org/10.1136/bmj.l6217.
[7] A.A. Tahami Monfared, M.J. Byrnes, L.A. White, Q. Zhang, The humanistic and economic burden of Alzheimer's disease, Neurol. Ther. 11 (2022) 525–551, https://doi.org/10.1007/s40120-022-00335-x.
[8] H. Shah, E. Albanese, C. Duggan, I. Rudan, K.M. Langa, M.C. Carrillo, K.Y. Chan, Y. Joanette, M. Prince, M. Rossor, et al., Research priorities to reduce the global burden of dementia by 2025, Lancet Neurol. 15 (2016) 1285–1294, https://doi.org/10.1016/S1474-4422(16)30235-6.
[9] Y.-L. Gao, N. Wang, F.-R. Sun, X.-P. Cao, W. Zhang, J.-T. Yu, Tau in neurodegenerative disease, 175–175, Ann. Transl. Med. 6 (2018), https://doi.org/10.21037/atm.2018.04.23.
[10] Hutton, M.; Lendon, C.L.; Rizzu, P.; Baker, M.; Froelich, S.; Houlden, H.; Pickering-Brown, S.; Chakraverty, S.; Isaacs, A.; Grover, A.; et al. Association of Missense and 5J-Splice-Site Mutations in Tau with the Inherited Dementia FTDP-17. 1998, 393, 4.
[11] R. Medeiros, D. Baglietto-Vargas, F.M. LaFerla, The role of tau in Alzheimer's disease and related disorders: role of tau in AD and related disorders, CNS Neurosci. Ther. 17 (2011) 514–524, https://doi.org/10.1111/j.1755-5949.2010.00177.x.
[12] K. Iqbal, F. Liu, C.-X. Gong, I. Grundke-Iqbal, Tau in Alzheimer disease and related tauopathies, Curr. Alzheimer Res. 7 (2010) 656–664, https://doi.org/10.2174/156720510793611592.
[13] M.D. Weingarten, A.H. Lockwood, S.Y. Hwo, M.W. Kirschner, A protein factor essential for microtubule assembly, Proc. Natl. Acad. Sci. 72 (1975) 1858–1862, https://doi.org/10.1073/pnas.72.5.1858.
[14] Iqbal, K.; del C. Alonso, A.; Gong, C.-X.; Khatoon, S.; Pei, J.-J.; Wang, J.Z.; Grundke-Iqbal, I. Mechanisms of Neurofibrillary Degeneration and the Formation of Neurofibrillary Tangles. In Ageing and Dementia; Jellinger, K., Fazekas, F.,

Windisch, M., Eds.; Journal of Neural Transmission. Supplementa; Springer Vienna: Vienna, 1998; Vol. 53, pp. 169–180 ISBN 978–3-211–83114-4.
[15] K. Iqbal, T. Zaidi, G.Y. Wen, I. Grundke-Iqbal, P.A. Merz, S.S. Shaikh, H. M. Wisniewski, I. Alafuzoff, B. Winblad, Defective brain microtubule assembly in Alzheimer's Disease, Lancet 2 (1986) 421–426.
[16] Y. Zhou, J. Shi, D. Chu, W. Hu, Z. Guan, C.-X. Gong, K. Iqbal, F. Liu, Relevance of phosphorylation and truncation of tau to the etiopathogenesis of Alzheimer's Disease, Front. Aging Neurosci. 10 (2018) 27, https://doi.org/10.3389/fnagi.2018.00027.
[17] H. Braak, E. Braak, I. Grundke-Iqbal, K. Iqbal, Occurrence of neuropil threads in the senile human brain and in Alzheimer's disease: a third location of paired helical filaments outside of neurofibrillary tangles and neuritic plaques, Neurosci. Lett. 65 (1986) 351–355, https://doi.org/10.1016/0304-3940(86)90288-0.
[18] R.J. O'Brien, P.C. Wong, Amyloid precursor protein processing and Alzheimer's disease, Annu. Rev. Neurosci. 34 (2011) 185–204, https://doi.org/10.1146/annurev-neuro-061010-113613.
[19] J.A. Hardy, G.A. Giggins, Alzheimer's disease: the amyloid cascade hypothesis, Science 256 (1992) 184–185, https://doi.org/10.1126/science.1566067.
[20] R. Ismail, P. Parbo, L.S. Madsen, A.K. Hansen, K.V. Hansen, J.L. Schaldemose, P. L. Kjeldsen, M.G. Stokholm, H. Gottrup, S.F. Eskildsen, et al., The relationships between neuroinflammation, beta-amyloid and tau deposition in Alzheimer's disease: a longitudinal PET study, J. Neuroinflamm. 17 (2020) 151, https://doi.org/10.1186/s12974-020-01820-6.
[21] M.J. Pontecorvo, M.D. Devous, M. Navitsky, M. Lu, S. Salloway, F.W. Schaerf, D. Jennings, A.K. Arora, A. McGeehan, N.C. Lim, et al., Relationships between flortaucipir PET Tau binding and amyloid burden, clinical diagnosis, age and cognition, Brain (2017) aww334, https://doi.org/10.1093/brain/aww334.
[22] D.L. Sparks, R.J. Kryscio, M.N. Sabbagh, C. Ziolkowski, Y. Lin, C. Liebsack, S. Johnson-Traver, Tau is reduced in AD plasma and validation of employed ELISA methods, Am. J. Neurodegener. Dis. 1 (2012) 99–106.
[23] Y. Liu, H. Qing, Y. Deng, Biomarkers in Alzheimer's disease analysis by mass spectrometry-based proteomics, Int. J. Mol. Sci. 15 (2014) 7865–7882, https://doi.org/10.3390/ijms15057865.
[24] A. Hye, J. Riddoch-Contreras, A.L. Baird, N.J. Ashton, C. Bazenet, R. Leung, E. Westman, A. Simmons, R. Dobson, M. Sattlecker, et al., Plasma proteins predict conversion to dementia from prodromal disease, e2, Alzheimers Dement 10 (2014) 799–807, https://doi.org/10.1016/j.jalz.2014.05.1749.
[25] M. Ameri, Z. Shabaninejad, A. Movahedpour, A. Sahebkar, S. Mohammadi, S. Hosseindoost, M.S. Ebrahimi, A. Savardashtaki, M. Karimipour, H. Mirzaei, Biosensors for detection of tau protein as an alzheimer's disease marker, Int. J. Biol. Macromol. 162 (2020) 1100–1108, https://doi.org/10.1016/j.ijbiomac.2020.06.239.
[26] C. Toyos-Rodríguez, F.J. García-Alonso, A. de la Escosura-Muñiz, ElectrochemicaL biosensors based on nanomaterials for early detection of Alzheimer's disease, Sensors 20 (2020) 4748, https://doi.org/10.3390/s20174748.
[27] A. de la Escosura-Muñiz, A. Merkoçi, Nanochannels preparation and application in biosensing, ACS Nano 6 (2012) 7556–7583, https://doi.org/10.1021/nn301368z.
[28] A. de la Escosura-Muñiz, A. Merkoçi, Nanochannels for electrical biosensing, TrAC Trends Anal. Chem. 79 (2016) 134–150, https://doi.org/10.1016/j.trac.2015.12.003.
[29] W.H. Coulter, High speed automatic blood cell counter and cell size analyzer, Proc. Natl. Electron Conf. 12 (1956) 1034–1040.
[30] S.M. Bezrukov, I. Vodyanoy, V.A. Parsegian, Counting polymers moving through a single ion channel, Nature 370 (1994) 279–281.
[31] H. Bayley, P.S. Cremer, Stochastic sensors inspired by biology, Nature 413 (2001) 226–230, https://doi.org/10.1038/35093038.
[32] H. Bayley, Membrane-protein structure: piercing insights, Nature 459 (2009) 651–652, https://doi.org/10.1038/459651a.
[33] Z.S. Siwy, S. Howorka, Engineered voltage-responsive nanopores, Chem. Soc. Rev. 39 (2010) 1115–1132, https://doi.org/10.1039/B909105J.
[34] A. Santos, T. Kumeria, D. Losic, Nanoporous anodic aluminum oxide for chemical sensing and biosensors, TrAC Trends Anal. Chem. 44 (2013) 25–38, https://doi.org/10.1016/j.trac.2012.11.007.
[35] A. de la Escosura-Muñiz, A. Merkoçi, Label-free voltammetric immunosensor using a nanoporous membrane based platform, Electrochem. Commun. 12 (2010) 859–863, https://doi.org/10.1016/j.elecom.2010.04.007.
[36] A. de la Escosura-Muñiz, A. Merkoçi, Nanoparticle based enhancement of electrochemical DNA hybridization signal using nanoporous electrodes, Chem. Commun. 46 (2010) 9007–9009, https://doi.org/10.1039/c0cc02683b.
[37] A. Iglesias-Mayor, O. Amor-Gutiérrez, C. Toyos-Rodríguez, A. Bassegoda, T. Tzanov, A. de la Escosura-Muñiz, Electrical monitoring of infection biomarkers in chronic wounds using nanochannels, Biosens. Bioelectron. 209 (2022), 114243, https://doi.org/10.1016/j.bios.2022.114243.
[38] A. de la Escosura-Muñiz, M. Espinoza-Castañeda, A. Chamorro-García, Rodríguez-Hernández, J. Carlos, C. de Torres, A. Merkoçi, In situ monitoring of PTHLH secretion in neuroblastoma cells cultured onto nanoporous membranes, Biosens. Bioelectron. 107 (2018) 62–68, https://doi.org/10.1016/j.bios.2018.01.064.
[39] A. de la Escosura-Muniz, K. Ivanova, T. Tzanov, Electrical evaluation of bacterial virulence factors using nanopores, ACS Appl. Mater. Interfaces 11 (2019) 13140–13146, https://doi.org/10.1021/acsami.9b02382.
[40] L. Zhou, H. Ding, F. Yan, W. Guo, B. Su, Electrochemical detection of Alzheimer's disease related substances in biofluids by silica nanochannel membrane modified glassy carbon electrodes, Analyst 143 (2018) 4756–4763, https://doi.org/10.1039/C8AN01457D.
[41] A. de la Escosura-Muñiz, A. Merkoçi, A nanochannel/nanoparticle-based filtering and sensing platform for direct detection of a cancer biomarker in blood, Small 7 (2011) 675–682, https://doi.org/10.1002/smll.201002349.
[42] W. Ye, Y. Xu, L. Zheng, Y. Zhang, M. Yang, P. Sun, A nanoporous alumina membrane based electrochemical biosensor for histamine determination with biofunctionalized magnetic nanoparticles concentration and signal amplification, Sensors 16 (2016) 1767, https://doi.org/10.3390/s16101767.
[43] A. de la Escosura-Muñiz, W. Chunglok, W. Surareungchai, A. Merkoçi, Nanochannels for diagnostic of thrombin-related diseases in human blood, Biosens. Bioelectron. 40 (2013) 24–31, https://doi.org/10.1016/j.bios.2012.05.021.
[44] Y. Wang, B. Sun, H. Wei, Y. Li, F. Hu, X. Du, J. Chen, Investigating immunosensor for determination of depression marker-Apo-A4 based on patterning AuNPs and N-Gr nanomaterials onto ITO-PET flexible electrodes with amplifying signal, Anal. Chim. Acta 1224 (2022), 340217, https://doi.org/10.1016/j.aca.2022.340217.
[45] Y.H. Tan, M. Liu, B. Nolting, J.G. Go, J. Gervay-Hague, G. Liu, A Nanoengineering Approach for Investigation and Regulation of Protein Immobilization, ACS Nano 2 (2008) 2374–2384, https://doi.org/10.1021/nn800508f.
[46] Y. Dong, C. Shannon, Heterogeneous immunosensing using antigen and antibody monolayers on gold surfaces with electrochemical and scanning probe detection, Anal. Chem. 72 (2000) 2371–2376, https://doi.org/10.1021/ac991450g.
[47] E.E. Congdon, J.E. Chukwu, D.B. Shamir, J. Deng, D. Ujla, H.B.R. Sait, T. A. Neubert, X.-P. Kong, E.M. Sigurdsson, Tau antibody chimerization alters its charge and binding, thereby reducing its cellular uptake and efficacy, EBioMedicine 42 (2019) 157–173, https://doi.org/10.1016/j.ebiom.2019.03.033.
[48] Å. Danielsson, A. Ljunglöf, H. Lindblom, One-step purification of monoclonal IgG antibodies from mouse ascites, J. Immunol. Methods 115 (1988) 79–88, https://doi.org/10.1016/0022-1759(88)90312-2.
[49] G.C. Ruben, K. Iqbal, I. Grundke-Iqbal, H.M. Wisniewski, T.L. Ciardelli, J. E. Johnson, The microtubule-associated protein tau forms a triple-stranded left-hand helical polymer, J. Biol. Chem. 266 (1991) 22019–22027, https://doi.org/10.1016/S0021-9258(18)54739-6.
[50] M. Kolarova, F. García-Sierra, A. Bartos, J. Ricny, D. Ripova, Structure and pathology of tau protein in Alzheimer disease, Int. J. Alzheimers Dis. 2012 (2012) 1–13, https://doi.org/10.1155/2012/731526.
[51] P. Weydt, L. Dupuis, Å. Petersen, Thermoregulatory Disorders in Huntington Disease. Handbook of Clinical Neurology 157, Elsevier, 2018, pp. 761–775. ISBN 978-0-444-64074-1.
[52] L. Ferrari, S.G.D. Rüdiger, Recombinant production and purification of the human protein tau, Protein Eng. Des. Sel. 31 (2018) 447–455, https://doi.org/10.1093/protein/gzz010.
[53] R. Brandt, N.I. Trushina, L. Bakota, Much more than a cytoskeletal protein: physiological and pathological functions of the non-microtubule binding region of Tau, Front. Neurol. 11 (2020), 590059, https://doi.org/10.3389/fneur.2020.590059.
[54] J. Luo, A. Sam, B. Hu, C. DeBruler, X. Wei, W. Wang, T.L. Liu, Unraveling PH dependent cycling stability of ferricyanide/ferrocyanide in redox flow batteries, Nano Energy 42 (2017) 215–221, https://doi.org/10.1016/j.nanoen.2017.10.057.
[55] S.C. Devanaboyina, S.M. Lynch, R.J. Ober, S. Ram, D. Kim, A. Puig-Canto, S. Breen, S. Kasturirangan, S. Fowler, L. Peng, et al., The effect of PH dependence of antibody-antigen interactions on subcellular trafficking dynamics, mAbs 5 (2013) 851–859, https://doi.org/10.4161/mabs.26389.
[56] T.T. Vu Nu, N.H.T. Tran, E. Nam, T.T. Nguyen, W.J. Yoon, S. Cho, J. Kim, K.-A. Chang, H. Ju, Blood-based immunoassay of tau proteins for early diagnosis of Alzheimer's disease using surface plasmon resonance fiber sensors, RSC Adv. 8 (2018) 7855–7862, https://doi.org/10.1039/C7RA11637C.
[57] O. Parlak, Portable and wearable real-time stress monitoring: a critical review, Sens. Actuators Rep. 3 (2021), 100036, https://doi.org/10.1016/j.snr.2021.100036.
[58] S. Schraen-Maschke, N. Sergeant, C.-M. Dhaenens, S. Bombois, V. Deramecourt, M.-L. Caillet-Boudin, F. Pasquier, C.-A. Maurage, B. Sablonnière, E. Vanmechelen, et al., Tau as a biomarker of neurodegenerative diseases, Biomark. Med. 2 (2008) 363–384, https://doi.org/10.2217/17520363.2.4.363.
[59] M.L. Chiu, W. Lawi, S.T. Snyder, P.K. Wong, J.C. Liao, V. Gau, Matrix effects—a challenge toward automation of molecular analysis, J. Assoc. Lab. Autom. 15 (2010) 233–242, https://doi.org/10.1016/j.jala.2010.02.001.
[60] J.-F. Masson, Consideration of sample matrix effects and "Biological" noise in optimizing the limit of detection of biosensors, ACS Sens 5 (2020) 3290–3292, https://doi.org/10.1021/acssensors.0c02254.

Celia Toyos-Rodríguez received her BSc in Biotechnology in 2017 at the University of Oviedo (Spain). She is now a PhD Student in the NanoBioAnalysis group, Department of Physical and Analytical Chemistry, University of Oviedo under a Pre-doctoral Researcher (FPI) grant. Her research interests focus on the development of electrochemical sensors based on nanomaterials for clinical diagnosis of Alzheimer's Disease and infection.

Francisco Javier García-Alonso received his PhD in Chemical Sciences in 1982 from the University of Valladolid (Spain). He is Full Professor in Inorganic Chemistry at the University of Oviedo (Spain) since 2009. His research interests focus on the synthesis of novel inorganic nanomaterials for applications in biosensing.

Alfredo de la Escosura-Muñiz holds a PhD in Chemistry (2006) from the University of Oviedo (Spain). As of June 2018 he holds a "Ramon y Cajal" Research Fellowship in the Nanobioanalysis Group, Department of Physical and Analytical Chemistry, University of Oviedo, where he is also a Lecturer in Chemistry. His research interests focus on the

development of biosensing systems based on nanoparticles and nanochannels for point-of-care diagnostic applications.